Available online at www.sciencedirect.com
SCIENCE DIRECT®
International Journal of Mass Spectrometry 229 (2003) 11–17
International Journal of Mass Spectrometry
www.elsevier.com/locate/ijms

Met-Cars: mass deposition and preliminary structural study via TEM

L. Gao [a], M.E. Lyn [a], D.E. Bergeron [a], A.W. Castleman Jr. [b,*]

[a] *Department of Chemistry, The Pennsylvania State University, University Park, PA 16802, USA*
[b] *Departments of Chemistry and Physics, The Pennsylvania State University, University Park, PA 16802, USA*

Received 20 December 2002; accepted 4 March 2003

Abstract

Transition metal–carbon clusters, including metallocarbohedrenes (Met-Cars), are of great interest for their potential applications in nanodevices. Herein we provide evidence of cluster-assembled nanoscopic features formed by the mass-gated deposition of large metal–carbon clusters. Gas phase zirconium–carbon species, gated at the mass corresponding to the Met-Car composition (M_8C_{12}), were deposited onto carbon-covered grids under both hard- and soft-landing conditions. The resulting deposited materials were analyzed via high-resolution transmission electron microscopy (HRTEM). Hard-landing conditions were found to lead to the production of species having a structure corresponding to the well-known bulk metal carbide, while studies of soft-landed deposits of zirconium Met-Cars were found to form a FCC structure with lattice parameter ∼15 Å, thus indicating cluster assembly.

Keywords: Metallocarbohedrenes (Met-Cars); Laser vaporization; Mass deposition; High-resolution transmission electron microscope (HRTEM)

1. Introduction

In 1992, we reported the discovery of a unique class of metal–carbon species composed of early transition metals bound to carbon in the stoichiometry M_8C_{12}, where M denotes the transition metals Ti, V, Hf, Zr and Nb [1]. These molecular clusters are termed metallocarbohedrenes, or Met-Cars for short. Subsequent work showed the existence of several other members of the family [2] as well as the facile formation of mixed metal Met-Cars [3]. Soon thereafter, we demonstrated the ability to produce Met-Cars in the solid state, but only as a component of a mixed soot system [4]. The unsuccessful search for a solvent capable of isolating the clusters has impeded progress in characterizing the material in the condensed state and, in contrast to the bulk carbides [5,6], these new nanoscale materials are under-explored [7].

Most of our knowledge about the properties of Met-Cars is based on gas phase studies; indeed numerous experimental and theoretical studies have been directed to investigations of their chemical [8,9] and geometrical [10–14] properties. A recent experimental investigation into the stability of individual neutral Met-Cars indicated that the species are very stable [15], and more recently, a theoretical study directed towards elucidating the nature of Met-Cars existing in the condensed phase shows two Met-Cars can be bound by ∼4.8 eV across four metal–carbon bonds [16] or can become bonded into a FCC lattice network [17]. The structure of the individual Met-Car differs from that of the conventional rock-salt carbide, and grows via a cage-like geometry under appropriate conditions [1c,15a,18].

Structures with a variety of bonding motifs have been considered theoretically to account for the Met-Cars' stability, with more recent experiments and theory tending to support a T_d structure rather than one with the originally proposed T_h symmetry [1] (for extensive review of experimental and theoretical Met-Car studies see [11,15b]). A very recent calculation has established that the C_{3v} structure has the lowest energy among the variants considered [14].

In view of difficulties in finding a suitable solvent for isolating Met-Cars, an alternative method involving the deposition of mass-gated species was employed in the present study. The experiments reported in this paper were conducted to produce Met-Cars from the direct laser vaporization (DLV) of metal/graphite composite pellets. After being mass gated and deposited onto carbon-covered grids, the resultant specimens were loaded onto the high-resolution

* Corresponding author. Tel.: +1-814-865-7242; fax: +1-814-865-5235.
E-mail address: awc@psu.edu (A.W. Castleman Jr.).

1387-3806/$ – see front matter © 2003 Elsevier B.V. All rights reserved.
doi:10.1016/S1387-3806(03)00250-1

transmission electron microscope (HRTEM)[1] for electron diffraction studies. Results from the first studies of deposits from mass gated Zr-Met-Cars using a reflectron equipped time-of-flight mass spectrometer are presented herein.

2. Experimental

The Met-Car clusters are produced from the DLV of metal/graphite pellets and studied using a time-of-flight mass spectrometer. The ion packet distribution is mass gated at the Met-Car cluster and deposited onto TEM grids under either hard- or soft-landing conditions. In the latter, a reflectron is employed to slow the ions prior to their deposition onto TEM grids placed at the turning position, thereby enabling soft landing. Pressed pellet samples are employed as targets because they have been found to yield Met-Cars more reliably than powder samples [19].

2.1. Preparation of the metal/graphite composite pellets

Pellets are made by dividing portions of pressed rods of 2:3 Zr:C molar compositions from zirconium[2] (−325 mesh, 99%, Alfa Aesar) and graphite powders (1–2 μm, Aldrich Chemicals). The powders are mixed by stirring with a spatula until a visually homogeneous mixture is apparent, and are then pressed in a 7/32-in. diameter die. The die is prepared with an aerosol colloidal graphite lubricant comprised of graphite in isopropyl alcohol (Alfa Aesar), which aids in releasing the rod after it is pressed. A pair of steel strip heaters is used to heat the die to approximately 110 °C as a load of ∼2.5 tons is applied overnight with a Carver manual compressor. As the powder mixture settles over the course of the first hour, the press is adjusted so as to maintain 2.5 tons of applied load.

2.2. Direct laser vaporization

The production of Met-Cars is accomplished via a DLV process (see Fig. 1A). In conducting the experiments, the target material is placed in an Al_2O_3 ceramic crucible mounted perpendicular to the axis of the mass spectrometer and located ∼4.5 cm below the center of the extraction region of the time-of-flight mass spectrometer. Ablation of the pellet is accomplished with a fluence of ∼100 mJ/cm^2 using the second harmonic, 532 nm (∼7 ns duration), from a GCR-3 Nd:YAG laser operated at 10 Hz. The light is focused to a spot size of ∼2.5 mm using a 40 cm focal length lens. Both the laser focus spot and crucible are kept stationary. Approximately 90 μs after the ablation laser pulse, cations in the expanding plume are extracted for mass analysis by applying a set of fast rising, high voltage pulses to the time-of-flight acceleration grids using two separate Behlke HTS-81 switches. Ions are detected with a pair of micro-channel plates; generated ion currents pass through a homemade pre-amplifier (200 MHz at 0.5 V; 222 gain) and are collected and averaged with a 175 MHz LeCroy 9400A oscilloscope. Timing of the laser and the ion optics is accomplished using a 10 Hz home-built pattern generator.

2.3. Mass deflection and depositions

Prior to deposition, Met-Cars are mass gated using a pair of deflector plates (see Fig. 1B). The application of pulsed deflection plates as a mass gate has already been described elsewhere [19,20–22]. Here, a pair of deflector plates is located along the flight axis at a distance of 170 cm from the center of the extraction region and 66 cm before the approximate turn-around position inside the reflectron. A positive potential of 1.0 kV is applied to one plate while the other is maintained at ground potential. At the time the Zr-Met-Cars approach the gate, the plate at +1.0 kV is pulsed to ground within 150 ns using a Behlke HTS-51 switch. Only ions that arrive at the mass gate during the time both deflector plates are at ground potential continue along the flight axis of the mass spectrometer. The transient pulse remains at ground potential for ∼3 ms; therefore, in the present arrangements, the gated species include the Met-Cars as well as (comparatively smaller quantities of) any larger species extracted from the source region with the applied 2.5 kV electrostatic potential. Varying the time interval during which the high voltage potential on the mass gate plate is pulsed down to ground, affects the mass range that is effectively selected by the gate.

Before using the mass gate to select the metal–carbon species, a test study establishing the ability to mass select C_{70} was conducted using a sample of an approximate 75/25% composition of C_{60}/C_{70} mixed fullerenes (MER Corporation).

Mass selected metal–carbon clusters with kinetic energies <20 eV (soft landing) or ∼2.28 keV (hard landing) are deposited onto lacey carbon covered Cu grids (Electron Microscopy Sciences/Diatome U.S./Summers Optical). The carbon layer is amorphous, allowing for facile identification of deposited crystalline species, as well as minimizing the potential for any epitaxial growth processes. A schematic of the configuration used for the hard and soft-landing depositions is shown in Fig. 1C. For the hard-landing depositions, the TEM grids are grounded and positioned along the flight axis 4 mm beyond the mass gate (Fig. 1A). In this case, the mass-selected ions are deposited with energies corresponding to the extraction potential since they are never exposed to a retarding field. By contrast, for the soft-landing depositions, the TEM grids are positioned inside the reflectron at a location where the approximate turn-around potential occurs for the mass-selected species. In the present

[1] The TEM experiments were conducted with the assistance by Dr. J.G. Wang, Material Research Institute at Pennsylvania State University.

[2] The zirconium power was packed under water. To dry the metal, spectroscopic grade acetone was added to the wet metal and the solution was evaporated to dryness in a fume hood.

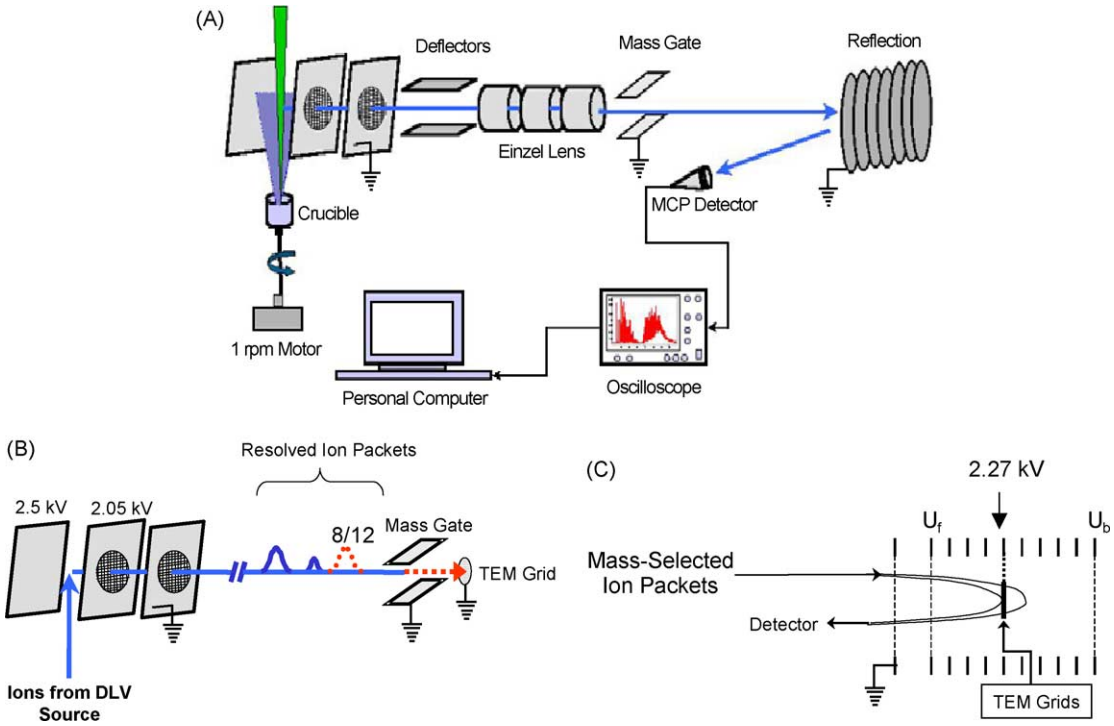

Fig. 1. Schematic of the newly constructed time-of-flight mass spectrometer. (A) The overall configuration, (B) hard-landing and (C) soft-landing deposition arrangements. Note that during the soft-landing deposition of the mass gated packets, the species are deposited with a small distribution of energies, arising from the spatial distribution in the extraction region of the time-of-flight.

experiments, this corresponds to ∼2.27 kV (Fig. 1B and C). Here, the ions are slowed significantly in the first stage of the reflectron and then linearly as they penetrate into the reflectron until they collide with the floating TEM grids at calculated energies <1 eV/atom. Hard- and soft-landing depositions were conducted for a total of ∼20 h over a 2- or 3-day period.

All species are exposed to air for short periods of time during the transfer from the mass spectrometer to the electron microscope. While Met-Cars have been found to be air sensitive under energetic collision conditions, they have been found to be stable for short exposure to air [4,8a,23]. Also, as discussed below, theoretical calculations suggest that the Met-Cars bond into a stable FCC structure in the condensed state. While elemental analysis indicated the presence of some oxygen on the grids, it should be noted that, upon careful analysis of the electron diffraction images, none of the diffraction features of the deposits described here were found to exhibit the crystalline characteristics of bulk oxides [24].

3. Results

Experiments were conducted under two deposition conditions. In one case the Zr/C system was studied under hard-landing conditions. Images of nanocrystals ∼20 Å in diameter could be seen from the hard-landing deposition of Zr/C species mass gated at Zr_8C_{12} (see Fig. 2A). No diffraction pattern could be obtained because the particles were too small. Due to the scale of the images, it is hard to quantitatively estimate the representative quality of the selected nanocrystals versus all nanocrystalline features on the grid surface. The features selected for detailed study were chosen for their amenability to fast Fourier transformation (FFT). Similar patterns were observed in some other spots in the images. Implementing the two-dimensional FFT [25] analysis of the images shown in Fig. 2A revealed *d*-spacings (Table 1) that correspond to the conventional rock-salt zirconium carbide [26]; see Fig. 2B. A limited number of diffraction spots (six at most) were extracted. These are indexed as belonging to two family planes, $(\bar{1}\,1\,1)(1\,\bar{1}\,\bar{1})(1\,\bar{1}\,1)(\bar{1}\,1\,\bar{1})$ and $(0\,0\,2)(0\,0\,\bar{2})$, associated with the [1 1 0] zone axis in a FCC lattice. As seen in the sketches (Fig. 2B) for these FFT results, the *d*-spacings are in good agreement with those reported in Table 1, which are obtained by calculation using Eq. (1) and are very close to the literature values [26] with less than 1% relative errors.

Following tests under hard-landing conditions, a soft-landing experiment was conducted for the Zr/C system using the arrangement in Fig. 1C. Soft-landed Zr/C species that were mass gated at Zr_8C_{12} are shown in Fig. 3A. A comprehensive set of diffraction spots with well-defined positions were indexed, yielding three sets of family planes: $(1\,\bar{1}\,3)(\bar{1}\,1\,\bar{3})$, $(\bar{3}\,1\,\bar{3})(3\,\bar{1}\,\bar{3})$ and $(\bar{4}\,2\,0)(4\,\bar{2}\,0)$, along with an unusually high order zone axis of [3 6 1] in a FCC lattice. In Table 2, it is seen that the relative ratios between *d*-spacings deviate from theoretical values by only 2.1% at

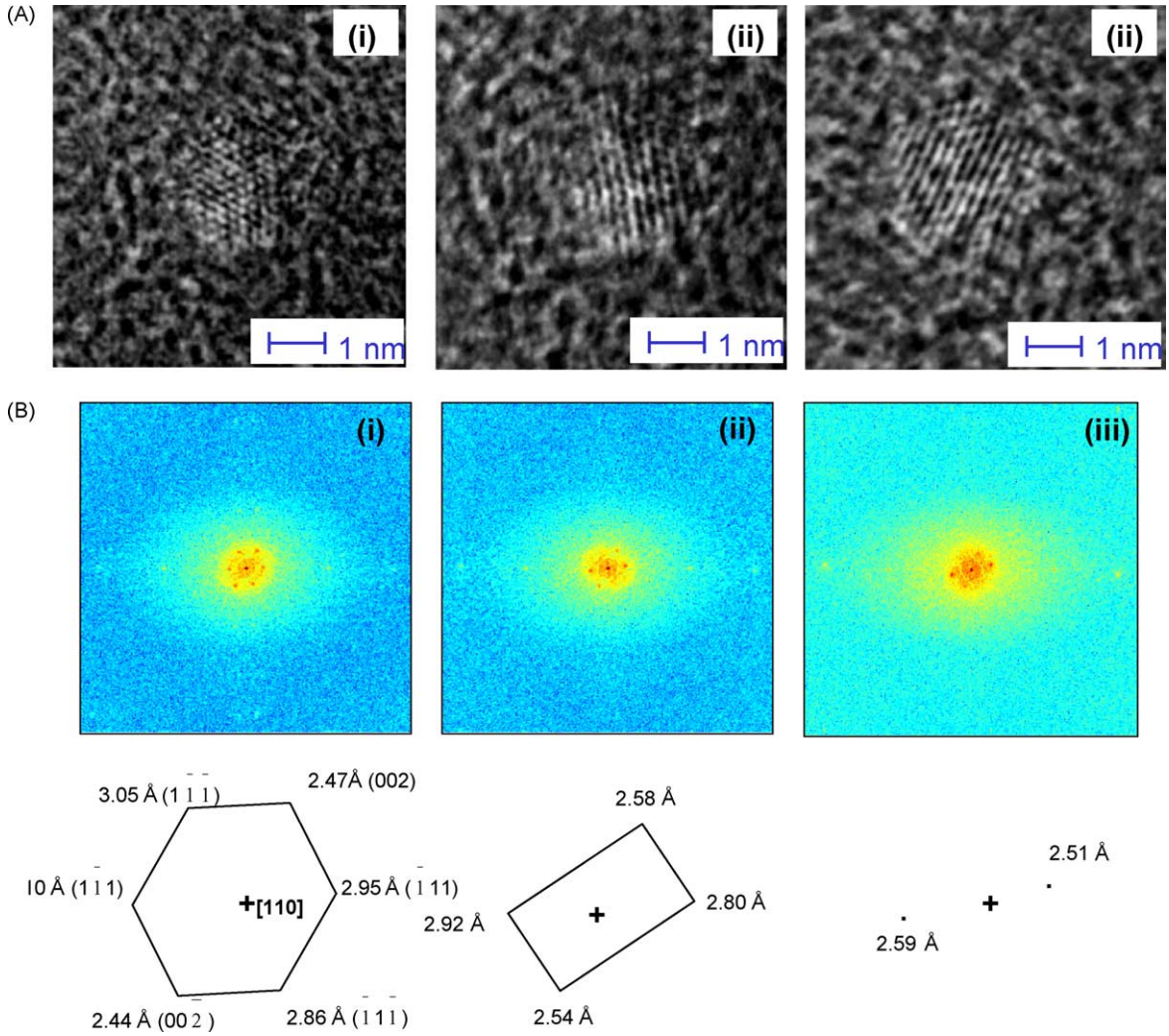

Fig. 2. The subparts (i), (ii), (iii) indicate images taken from different area in the TEM specimen: (A) HRTEM images of Zr/C deposits mass gated at Zr_8C_{12}. The species were deposited with ~2.28 kV of kinetic energy. (B) Two-dimensional fast Fourier transformations (FFT) of the images. The sketches show the *d*-spacings obtained from the FFT images that correspond to the above images, respectively. Errors associated with the FFT are evident from the asymmetry of the *d*-spacings shown in the sketches.

most. This indicates a great degree of certainty in indexing the diffraction spots. Three *d*-spacings, 4.666, 3.746 and 3.440 Å, could be determined from the diffraction pattern (Fig. 3B) obtained from a region in the image shown in Fig. 3A. These calculated *d*-spacings (Table 2) do not correspond to those of either ZrC or ZrO_2. The average value of the lattice parameter of the cubic unit cell is calculated to be 15.34 Å.

Table 1
Index results of hard-landing Zr/C system: along [1 1 0] zone axis

i	*h k l*[a]	R_i (mm) (reciprocal vector mode)	Image analysis data comparison	D_i (Å) (*d*-spacing value)	θ_{ri-r1}[b] (interplanar angle)	D_i/D_1 (spacing ratio)
1	1 1 1	3.41	Exp. value	2.95	70.9°	1
			Ref. value[c]	2.709	70.52°	1
			Relative error (%)	8.8	0.54	0
2	2 0 0	3.98	Exp. value	2.52	54.35°	1.168
			Ref. value[c]	2.346	54.74°	1.155
			Relative error (%)	7.5	−0.71	0.54

[a] The corresponding diffraction pattern obtained from computer simulation (not presented here) is in good agreement with the experimental pattern.
[b] $\theta_{ri-r1} = \cos^{-1}[(h_i\,k_i\,l_i)(h_1\,k_1\,l_1)/(h_i\,k_i\,l_i)^{1/2}(h_1\,k_1\,l_1)^{1/2}]$.
[c] ZrC powder diffraction data [26].

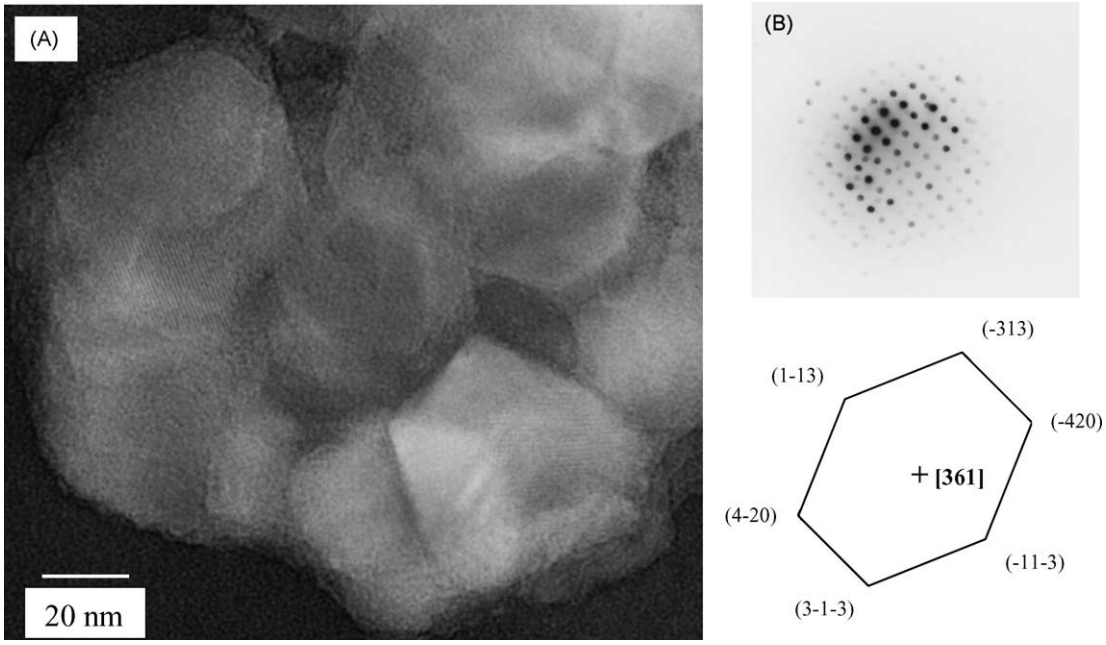

Fig. 3. HRTEM images of soft-landed Zr/C species mass gated at Zr_8C_{12} (A) and a corresponding diffraction pattern (B).

Table 2
Index results of soft-landing Zr/C system: along [3 6 1] zone axis

i	$h\,k\,l$[a]	R_i (mm) (reciprocal vector mode)	Image analysis data comparison	D_i (Å) (d-spacing value)	θ_{ri-r1}[b] (interplanar angle)	D_i/D_1 (spacing ratio)
1	3 1 1	2.15	Exp. value	4.67	68.0°	1
			Ref. value	N.A.	69.77°	1
			Relative error (%)	N.A.	0.54	0
2	3 3 1	2.89	Exp. value	3.48	68.0°	1.34
			Ref. value	N.A.	69.77°	1.314
			Relative error (%)	N.A.	2.5	2.1
3	4 2 0	2.98	Exp. value	3.44	66.0	1.36
			Ref. value	N.A.	66.14	1.348
			Relative error (%)	N.A.	0.21	0.6

[a] The corresponding diffraction pattern obtained from computer simulation (not presented here) is in good agreement with the experimental pattern.
[b] $\theta_{ri-r1} = \cos^{-1}[(h_i\,k_i\,l_i)(h_1\,k_1\,l_1)/(h_i\,k_i\,l_i)^{1/2}(h_1\,k_1\,l_1)^{1/2}]$.

4. Discussion

All experimental d-spacings presented in Tables 1 and 2 were calculated using the Bragg condition to a first-order approximation:

$$d \cong \lambda \frac{L}{r} \tag{1}$$

where λ, L, and r represent the wavelength of the electron beam, the diffraction camera length, and the measured distance between two lattice points or the radius of a Debye–Scherrer ring [27]. The experimental parameters L and λ are 400 mm and 0.00251 nm, respectively.

On the basis of the FFT results, we conclude that only the metal carbide species, ZrC, with a much simpler structure and smaller lattice parameter than expected for Met-Cars, are dominant in the TEM specimen produced under hard-landing conditions. The possibility of impact-stimulated formation of surface alloys as the mechanism responsible for the observed carbide bulk structure cannot be excluded [26,28]. In fact, it is considered likely that the clusters' collision energy could be transformed simultaneously into embedding energy *and*/*or* fragmentation energy, allowing the deposits to re-construct freely through interactions with the substrate. Evidently, under these conditions, the deposited Met-Cars and larger Zr/C species underwent atomic rearrangements to produce the conventional metal carbide, ZrC, instead of assemblies of Met-Cars or larger clusters.

Significantly, the image acquired under soft-landing conditions was quite different. Indeed, the Zr/C deposition revealed the presence of a species that may be Zr-Met-Cars (or possibly a composite with larger cluster assemblies)

Table 3
Lattice parameter calculation for "Zr-Met-Cars" cubit unit shown in Fig. 3B

d (Å) (d-spacing)	$h\,k\,l$ (Muller indices)	$(h^2 + k^2 + l^2)^{1/2}$	a (Å)[a] (lattice constant)
4.67	3 1 1	$(11)^{1/2}$	15.48
3.48	3 3 1	$(19)^{1/2}$	15.15
3.44	4 2 0	$(20)^{1/2}$	15.38
r (Å)[b] (size of packing ball) = 5.42		Average a (Å) = 15.34	

[a] The lattice constant a is calculated based on the formula: $a = d_{hkl} \times (h^2 + k^2 + l^2)^{1/2}$.
[b] The size of the packing unit is calculated based on the 'closet hard-sphere model' and the corresponding geometrical relationship between a and r: $4r = (2)^{1/2}a$.

displaying a substantially larger lattice parameter, namely 15.34 Å, than the cubic ZrC [26]. This value provides encouraging evidence for cluster assembly. It is important to note that whether through discharging, or through impact-induced structural rearrangement, it is possible that geometrical perturbations of the Met-Car structure might occur. However, as the structures for neutral and charged Met-Cars are not completely characterized, any such perturbations would be unobservable in the present experiments.

We note that there are moderately large differences between this value and those of Ti Met-Cars deduced from both a purely geometrical [29] and a theoretical [17] calculation (Tables 3 and 4). These differences likely arise, at least partially, because of the consideration discussed below.

Zirconium is located one row below titanium in group IV in the periodic table, with larger radii in both the 0 and +4 oxidation states than those of titanium (Table 5). When Zr and Ti participate in constructing a Met-Car structure, similar trends between the two structural parameters for the corresponding Met-Cars would be anticipated. This is in general agreement with the comparisons shown in Table 4, but with larger ratio values. A complete understanding of the differences brought about by the replacement of Ti by Zr must await structural calculations specific to the Zr-Met-Cars. Whether or not there should be a necessarily linear relationship of the radii between naked atoms or ions and Met-Cars is still an open question.

Table 4
Comparison of dimensions between "Ti-Met-Cars" and "Zr-Met-Cars"

Methods	Radius of Zr-Met-Cars (Å)	Radius of Ti-Met-Cars (Å)	Radii ratio
Calculation[a] [29]	3.65	2.30	1.6
Experimental (lattice parameter a)	5.42[a] (15.34)	N.A.	1.5
Theoretical[a] [17] (lattice parameter a)	N.A.	3.55[a] (10.04)	

[a] Calculation based on the relationship between a and r: $4r = (2)^{1/2}a$.

Table 5
Radii [30] comparison between titanium and zirconium

Oxidation state	Radius of Ti (Å)	Radius of Zr (Å)	Radii ratio
0	0.68	0.80	1.2
+4	1.49	1.60	1.1

Before drawing the final conclusion for the studies presented herein, we wish to point out some limitations in our study of using TEM to derive structural information on Met-Cars. Previous studies have concluded that Met-Cars usually behave like "giant" atoms. Inspired by this view, we assume that the cluster-assembled species in the TEM specimen examined in Fig. 3 scatters the oncoming electron beam as a "hard-sphere". This assumption serves to explain why our current TEM images alone cannot provide fine structure information regarding the arrangements of the individual metal and carbon atoms.

The second limitation lies in the intrinsic accuracy limit of TEM itself. Even with high quality data, usually TEM results alone cannot provide enough precision to fully characterize material structures. In most cases, TEM investigations should be used only as one complementary technique along with other measurements, such as X-ray diffraction and extended X-ray edge fine-structure analysis, to provide additional information, which could either support or refute the initial tentative characterization. Therefore, with only limited d-spacing values from the TEM image analysis, the data presented in this paper should only be taken as a preliminary study towards our ultimate goal: characterizing deposited Met-Cars and their assemblies.

5. Conclusions

The presented results indicate that, under hard-landing conditions, zirconium Met-Cars and larger metal–carbon species undergo atomic rearrangement to produce the respective metal carbide, while a significantly larger species packed in a FCC structure with a lattice parameter of 15.34 Å was found under soft-landing conditions. We cannot specifically ensure the deposits are comprised only of Met-Cars with the current experimental set-up; however, the large dimensions of the FCC lattice suggests cluster assembly.

The regular lattice of the deposited material is indicative of the assembly of uniform particles. The statistical distribution of clusters larger than Met-Cars seems an unlikely source for the building blocks of such a regular assembly. In addition, the clusters higher in mass than the Met-Cars are thought to have essentially nanocrystalline carbide structures. Intuitively, the coalescence of such clusters would yield features with lattice characteristics resembling bulk carbides. No such features were observed in the present study, and so it is tentatively suggested that the assemblies described here are likely composed mainly of Met-Cars. Further investigations with a narrower mass selection window will eventually allow direct comparison of carbide cluster and Met-Car deposit characteristics.

The results obtained thus far provide two prospects. First, the hard/soft-landing deposition method builds a bridge between the DLV coupled mass spectrometry and TEM as a tool for structural investigation. This combination yields a very valuable route to study some novel clusters that are initially observed in the gas phase and can neither be immediately synthesized nor isolated in the solid state in relatively large quantities. Secondly, the experimental conditions used in this preliminary investigation lay the foundation for a new platform for further studies aiming at producing Met-Car-based materials in macroscopic quantities and gaining insights into the interaction and arrangements of nanometric, caged carbide species (Met-Cars) on surfaces.

Acknowledgements

The authors would like to thank Professor Elizabeth Dickey of the Department of Materials Science and Engineering at Pennsylvania State University for the enlightening discussions regarding TEM image indexing and Jinguo Wang of the Materials Research Institute at the Pennsylvania State University for assistance in TEM imaging. Finally, we gratefully acknowledge financial support from the AFOSR, Grant No. F49620-01-1-0122 for the soft-landing studies and the NSF-NIRT, Grant No. DMR01-03585 for the hard-landing investigations.

References

[1] (a) B.C. Guo, K.P. Kerns, A.W. Castleman Jr., Science 255 (1992) 1411;
(b) B.C. Guo, S. Wei, J. Purnell, S.A. Buzza, A.W. Castleman Jr., Science 256 (1992) 515;
(c) S. Wei, B.C. Guo, J. Purnell, S.A. Buzza, A.W. Castleman Jr., J. Phy. Chem. 96 (1992) 4166;
(d) S. Wei, B.C. Guo, H.T. Deng, K. Kerns, J. Purnell, S.A. Buzza, A.W. Castleman Jr., J. Am. Chem. Soc. 116 (1994) 4475.
[2] (a) J.S. Pilgrim, M.A. Duncan, J. Am. Chem. Soc. 115 (1993) 6958;
(b) J.S. Pilgrim, M.A. Duncan, J. Am. Chem. Soc. 115 (1993) 9724.
[3] (a) S.F. Cartier, B.D. May, A.W. Castleman Jr., J. Chem. Phys. 100 (1994) 5384;
(b) S.F. Cartier, B.D. May, A.W. Castleman Jr., J. Am. Chem. Soc. 116 (1994) 5295;
(c) H.T. Deng, B.C. Guo, K.P. Kerns, A.W. Castleman Jr., Int. J. Mass Spectrom. Ion Process. 138 (1994) 275.
[4] S.F. Cartier, Z.Y. Chen, G.J. Walder, C.R. Sleppy, A.W. Castleman Jr., Science 260 (1993) 195.
[5] H.O. Pierson, Handbook of Refractory Carbides and Nitrides: Properties, Characteristics, Processing, and Applications, Noyes Publications, Park Ridge, NJ, 1996.
[6] T. Oyama, in: R.E. Kirk (Ed.), Encyclopedia of Chem. Tech., 1890–1957, 4th ed., Wiley, New York, 1991.
[7] S. McCarty, J.C. Love, J.G. Kushmerick, L.F. Charles, C.D. Keating, B.J. Toleno, M.E. Lyn, A.W. Castleman Jr., M.J. Natan, P.S. Weiss, J. Nanoparticle Res. 1 (4) (1999) 459.
[8] (a) B.C. Guo, K.P. Kerns, A.W. Castleman Jr., J. Am. Chem. Soc. 115 (1993) 7415;
(b) H.T. Deng, B.C. Guo, K.P. Kerns, A.W. Castleman Jr., J. Phys. Chem. 98 (1994) 13373;
(c) K.P. Kerns, B.C. Guo, H.T. Deng, A.W. Castleman Jr., J. Am. Chem. Soc. 117 (1995) 4026;
(d) H.T. Deng, K.P. Kerns, A.W. Castleman Jr., J. Am. Chem. Soc. 118 (1996) 446.
[9] (a) C.S. Yeh, Y.G. Byun, S. Afzaal, S.Z. Kan, S. Lee, B.S. Freiser, P.J. Hay, J. Am. Chem. Soc. 117 (1995) 4042;
(b) C.S. Yeh, S. Afzaal, S.A. Lee, Y.G. Byun, B.S. Freiser, J. Am. Chem. Soc. 116 (1994) 8806;
(c) Y.G. Byun, S.A. Lee, S.Z. Kan, B.S. Freiser, J. Phys. Chem. 100 (1996) 14281;
(d) Y.G. Byun, B.S. Feiser, J. Am. Chem. Soc. 118 (1996) 3681.
[10] (a) I. Dance, J. Chem. Soc., Chem. Commun. 1992, 1779;
(b) I. Dance, J. Am. Chem. Soc. 118 (1996) 6309.
[11] M.-M. Rohmer, M. Benard, J.-M. Poblet, Chem. Rev. 100 (2000) 495.
[12] (a) D. van Heijnsbergen, G. von Helden, M.A. Duncan, A.J.A. van Roij, G. Meijer, Phys. Rev. Letts. 83 (1999) 4983;
(b) D. van Heijnsbergen, M.A. Duncan, G. Meijer, G. von Helden, Chem. Phys. Letts. 349 (2001) 220.
[13] G.K. Gueorguiev, J.M. Pacheco, Phys. Rev. Letts. 88 (2002) 115504.
[14] T. Baruah, M.R. Pederson, M.E. Lyn, A.W. Castleman Jr., Phys. Rev. A 66 (2002) 053201.
[15] (a) H. Sakurai, A.W. Castleman Jr., J. Phys. Chem. A 101 (1997) 7695;
(b) H. Sakurai, A.W. Castleman Jr., J. Phys. Chem. A 102 (1998) 10486.
[16] T. Baruah, M.R. Pederson, Phys. Rev. B 66 (2002) 241404.
[17] Scientific communication with J.J. Zhao at the University of North Carolina.
[18] (a) S. Wei, B.C. Guo, J. Purnell, S. Buzza, A.W. Castleman Jr., Science 256 (1992) 818;
(b) S. Wei, A.W. Castleman Jr., Chem. Phys. Lett. 227 (1994) 305.
[19] M.E. Lyn, Ph.D. thesis, Chemistry Department at Pennsylvania State University, 2002.
[20] K.D. Rinner, D.A. Kliner, R.S. Blake, R.N. Zare, Rev. Sci. Instrum. 60 (1989) 717.
[21] D.S. Cornett, M. Peschke, K. LaiHing, P.Y. Cheng, K.F. Wiley, M.A. Duncan, Rev. Sci. Instrum. 63 (1992) 2177.
[22] H. Haberland, H. Kornmeier, C. Ludewigt, A. Risch, Rev. Sci. Instrum. 62 (11) (1991) 2368.
[23] H.T. Deng, K.P. Kerns, R.C. Bell, A.W. Castleman Jr., Int. J. Mass Spectrom. Ion Process. 167/168 (1997) 615.
[24] File No. 27-997, 37-31, 20-684, Powder Diffraction File, published by the International Centre for Diffraction Data, 1601 Park Lane, Swarthmore, PA.
[25] Program *Matlab* from Mathsoft (matrix laboratory http://www.mathsoft.com).
[26] File No. 35-784, Powder Diffraction File, published by the International Centre for Diffraction Data, 1601 Park Lane, Swarthmore, PA.
[27] L. Reimer, Transmission Electron Microscopy, 3rd ed., Springer-Verlag, Berlin, 1993.
[28] B. Pauwels, G.V. Tendeloo, W. Bouwen, L.T. Kuhn, P. Lievens, H. Lei, M. Hou, Phys. Rev. B 62 (15) (2000) 10383.
[29] Castleman group member, J. Stairs.
[30] Handbook of Chemistry and Physics, 1954–1955, 36th ed., Chemical Rubber Publishing Co., Cleveland, OH.